Quantitative structural imaging of keratoconic corneas using polarization-resolved SHG microscopy

Clothilde Raoux, Margaux Schmeltz, Marion Bied, Maged Alnawaiseh, Uwe Hansen, Gaël Latour, Marie-Claire Schanne-Klein

Research Article | Vol. 12, No. 7 / 1 July 2021 / Biomedical Optics Express 4163
Biomedical Optics EXPRESS

Quantitative structural imaging of keratoconic corneas using polarization-resolved SHG microscopy

CLOTHILDE RAOUX,[1,5] MARGAUX SCHMELTZ,[1,5] MARION BIED,[1] MAGED ALNAWAISEH,[2] UWE HANSEN,[3] GAËL LATOUR,[1,4] AND MARIE-CLAIRE SCHANNE-KLEIN[1,*]

[1]*Laboratory for Optics and Biosciences, Ecole polytechnique, CNRS, INSERM, Institut Polytechnique de Paris, 91128 Palaiseau, France*
[2]*Department of Ophthalmology, Hospital Fulda, University of Marburg, Campus Fulda, 36043 Fulda, Germany*
[3]*Institute for Musculoskeletal Medicine, University Hospital Münster, 48149 Münster, Germany*
[4]*Université Paris-Saclay, 91190 Saint-Aubin, France*
[5]*These authors contributed equally*
[*]*marie-claire.schanne-klein@polytechnique.edu*

Abstract: The human cornea is mainly composed of collagen fibrils aligned together within stacked lamellae. This lamellar structure can be affected in pathologies such as keratoconus, which is characterized by progressive corneal thinning and local steepening. In this study, we use polarization-resolved second harmonic generation (P-SHG) microscopy to characterize 8 control and 6 keratoconic human corneas. Automated processing of P-SHG images of transverse sections provides the collagen orientation in every pixel with sub-micrometer resolution. Series of P-SHG images recorded in the most anterior region of the stroma evidence sutural lamellae inclined at 22° ± 5° to the corneal surface, but show no significant difference between control and keratoconic corneas. In contrast, series of P-SHG images acquired along the full thickness of the stroma show a loss of order in the lamellar structure of keratoconic corneas, in agreement with their defective mechanical properties. This structural difference is analyzed quantitatively by computing the entropy and the orientation index of the collagen orientation distribution and significant differences are obtained along the full thickness of the stroma. This study shows that P-SHG is an effective tool for automatic quantitative analysis of structural defects of human corneas and should be applied to other collagen-rich tissues.

1. Introduction

The human cornea exhibits a highly organized structure that is crucial to ensure its main physiological functions, namely maintenance of ocular integrity, transparency and refraction. The corneal stroma, which represents 90% of the cornea thickness, is composed of 1–3 µm thick stacked lamellae that run roughly parallel to the cornea surface and are mainly oriented along two perpendicular directions in the center of the cornea [1]. These lamellae are constituted of well-aligned thin collagen fibrils (30 nm diameter) within a non fibrillar matrix composed of proteoglycans, glycosaminoglycans and other biopolymers. The precise distribution and shape of these lamellae along the depth and the radial extent of the cornea as well as the distribution and number of Vogt striae, which correspond to local undulations of these lamellae, are a matter of many investigations [2–7]. Nonetheless, it is well established that the cornea lamellar structure is a key factor in the mechanical properties of the cornea [8–10]. It enables the cornea to maintain its physiological curvature and thus its refractive power despite daily variations in the intraocular pressure and applications of external forces, such as eye rubbing or physical shocks [1,10].

#426145 https://doi.org/10.1364/BOE.426145
Journal © 2021 Received 30 Mar 2021; revised 29 Apr 2021; accepted 22 May 2021; published 16 Jun 2021

Biomedical Optics EXPRESS

Keratoconus is a corneal pathology, which affects approximately 15/10000 persons [11]. It is characterized by progressive corneal thinning, local steepening and formation of a cone. Vision is thus strongly impaired and in the most advanced cases of keratoconus, a corneal graft is needed. Keratoconic corneas also exhibit a defective mechanical behavior, as measured routinely by clinical devices such as the Reichert Ocular Response Analyzer [12]. Accordingly, many studies have characterized the ultrastructure and the structure of keratoconic corneas and evidenced a distortion of the stroma lamellar organization [13–21].

Notably, Second Harmonic Generation (SHG) microscopy has proven to be an effective method to compare the structure of healthy and keratoconic human corneas. Indeed, this technique reveals specifically unstained collagen fibrils with an excellent contrast. As a multiphoton mode of contrast, it also provides three-dimensional capability and enables micrometer-scale imaging of the full depth of intact corneas [22,23]. Accordingly, SHG microscopy has been used to assess the collagen lamellae organization of keratoconic corneas both in transverse sections and in intact corneas using *en-face* imaging [16–20]. However, as a complex coherent nonlinear signal, SHG is highly sensitive to the collagen distribution within the focal volume [24–27], which hinders the quantitative analysis of SHG images in dense collagen-rich tissues. Moreover, the determination of the collagen orientation directly by image processing of the SHG data degrades the resolution because several neighboring pixels need to be considered to assess the orientation in every pixel. Accordingly, a refinement of the SHG technique is needed to provide a reliable quantitative assessment of the lamellar orientation distribution in the full stroma.

This study aims at quantifying the distribution of lamellae orientations along the full thickness of control and keratoconic corneas in an automatic unbiased way. We use polarization-resolved SHG (P-SHG) microscopy that advantageously combines the specificity of SHG imaging for collagen fibrils with the sensitivity of polarimetric techniques to submicrometer-scale anisotropy [24,25,28,29]. It consists in recording a series of SHG images using various orientations of a linearly-polarized excitation beam. Appropriate data processing based on a tensorial analysis of the collagen SHG signal then provides the orientation of the collagen fibrils in every pixel. While P-SHG microscopy has already been performed in corneas [9,30,31], this technique has never been used to quantify lamellae disorganization in keratoconic corneas.

In this paper, we use transmission electron microscopy (TEM) and P-SHG to characterize transverse sections of control and keratoconic corneas. We implement an automated analysis of the orientation distributions obtained from P-SHG images to quantify the orientation disorder of the stromal lamellae. Our results show a structural difference between control and keratoconic corneas and confirm a loss of order in the lamellar structure of keratoconic corneas.

2. Materials and methods

2.1. Human cornea samples

The study was carried out according to the tenets of the Declaration of Helsinki and followed ethical requirements for human tissues. 8 control and 6 keratoconic human corneas were obtained from the Department of Ophthalmology of the University Hospital of Münster Medical Center, with permission by the ethics committee Münster (2017-106-f-S). Authorization to handle human corneas at LOB was obtained from the French administration (CODECOH agreement DC-2018-3300). The control corneas were collected post-mortem with the limbus and the sclera. The keratoconic corneas were corneal buttons without limbus obtained as surgical excisions from patients with stage 3 keratoconus, showing significant corneal scarring and reduced visual acuity.

The corneas were fixed in 2% (v/v) formaldehyde and 2.5% (v/v) glutaraldehyde in 100 mM cacodylate buffer, pH=7.4, at 4°C overnight. After washing in PBS, corneas were cut in small pieces and post-fixed in 0.5% (v/v) osmiumtetroxide and 1% (w/v) potassium hexacyanoferrate (III) in 0.1 M cacodylate buffer for 2 h at 4°C, followed by washing with distilled water. After dehydration in an ascending ethanol series from 30 to 100% ethanol, specimens were two times

Biomedical Optics EXPRESS

incubated in propylenoxide each for 15 min and embedded in Epon. 70 nm- and 2 µm-thick transverse sections were cut with an ultramicrotome through or very close to the apex and orientated with respect to the epithelium. The 70 nm-thick sections were collected on copper grids and negatively stained with 2% uranyl acetate for 15 min for TEM imaging. The 2 µm-thick sections were collected on coverslips and dried at 37°C on a heating plate, and remained unstained for SHG imaging. This method advantageously provides ultrathin and thin transverse sections from the same region of the cornea, which enables reliable comparison of the electron micrographs and the SHG images. Moreover, thanks to the Epon embedding that keeps the cornea hard and prevents any tissue distortion during cutting, the stromal structure is well-preserved in the thin sections [32].

2.2. Transmission electron microscopy

Transmission electron micrographs were taken at 60 kV with a Philips EM-410 electron microscope using imaging plates (Ditabis, Pforzheim, Germany). Electron micrographs were taken from different positions on the ultrathin sections. The epithelium and/or endothelium were used for determination of the location of every electron micrographs.

2.3. Polarization-resolved SHG microscopy

SHG images were recorded by use of a custom-built upright laser scanning multiphoton microscope as previously described [33]. Excitation was provided by a femtosecond Titanium-Sapphire laser (Mai-Tai, Spectra-Physics) tuned at 860 nm and scanned in the XY directions using galvanometric mirrors. A high numerical aperture (NA) objective lens with water immersion (25x, NA 1.05, Plan-Apochromat, Olympus) was used to achieve resolutions of approximately 0.4 µm (lateral) x 1.2 µm (axial) and a field of view of 540×540 µm^2. Power at the sample was 5 to 12 mW with 10 µs pixel dwell time. SHG signals were detected in the trans-direction through a condenser (effective NA≈1.4) by means of a photon-counting photomultiplier tube (P25PC, Electron tubes) and suitable spectral filters to reject the excitation beam and select the second harmonic signal at 430 nm (FF01-680SP, FF01-720SP, FF01-427/10 Semrock).

Polarization-resolved SHG images (P-SHG) were obtained by recording series of SHG images excited by linearly polarized incident electric fields with different orientations. The orientation of the incident field polarization was controlled by two waveplates inserted at the back aperture of the objective. The ellipticity, defined as the ratio of the minimal to maximal electric fields, was smaller than 4% for every polarization. Series of 18 images were acquired every 10° between 0° and 170° (alternatively 24 images every 15° between 0° and 345°).

2 sets of P-SHG data were acquired on all human cornea transverse sections (Fig. 1(a)). The first dataset focused on the most anterior region of the stroma, close to the epithelium. It was composed of series of P-SHG images with 210 nm pixel size spanning the full width of the cornea section (Fig. 1(b)). 2 to 12 P-SHG images (tiles) of 150×80 µm^2 size were recorded, depending on the size of every transverse section. These tiles were then stitched together to get a wide high-resolution P-SHG image of the most anterior region of the stroma. The second dataset focused on the full thickness of the stroma. It was composed of series of P-SHG images with 420 nm pixel size spanning the full thickness of the cornea from the epithelium to the endothelium. These tiles were then stitched together to get a P-SHG image showing the anterior, middle and posterior regions of the stroma (Fig. 1(c)).

2.4. Theoretical analysis and numerical processing of P-SHG data

The SHG signal of a collagen fibril must be described in the theoretical framework of tensorial nonlinear optics [34]. It depends on 3 types of parameters:

Biomedical Optics EXPRESS

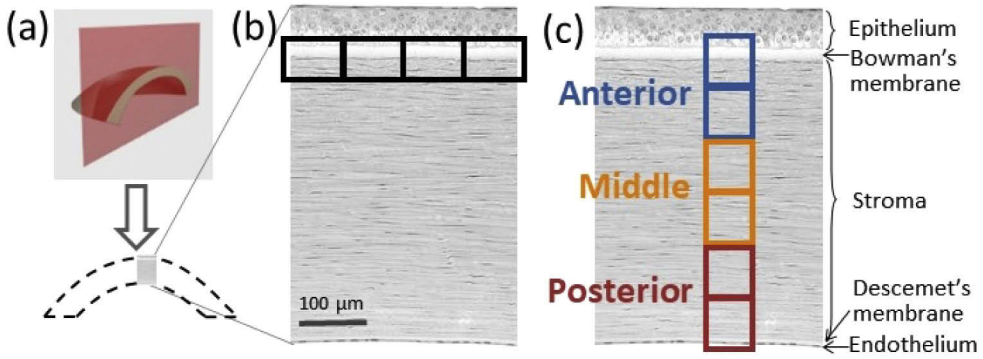

Fig. 1. Location of P-SHG images. (a) Scheme of cornea transverse section. (b) First set of P-SHG images spanning the most anterior region of the stroma. (c) Second set of P-SHG images on the full thickness of the stroma. Each rectangle in (b) and (c) corresponds to a P-SHG tile.

1. the polarization and the intensity I_{exc} of the laser excitation at frequency ω (Fig. 2(a)). In this study, we consider linear polarizations that are parametrized by their angle θ to the laboratory X axis.

2. the orientation of the collagen fibril in the laboratory frame (Fig. 2(b)): the angle φ in the imaging plane XY and the angle ψ out of the imaging plane. Since the collagen lamellae in the corneal stroma are composed of well-aligned fibrils, we consider here that all the collagen fibrils within the focal volume have the same orientation, in contrast to more complex approaches that introduce sub-micrometer orientation disorder. Note that P-SHG is not sensitive to the polarity of collagen fibrils, like usual linear polarimetry, so that the φ and ψ angles are defined in smaller ranges than Euler angles: $\varphi, \psi \in]-90°, +90°]$.

3. the second harmonic response of the collagen fibrils that is described by a susceptibility tensor $\chi^{(2)}$. We assume as in previous reports that this tensor exhibits a cylindrical symmetry in the fibril frame (xyz), with x the fibril direction, and that the Kleinman symmetry applies [28,35]. While more complex tensors may be used, these assumptions have been shown to well reproduce experimental P-SHG data and to limit the number of independent tensor components to only 2: $\chi^{(2)}_{xxx}$ and $\chi^{(2)}_{xyy} = \chi^{(2)}_{xzz} = \chi^{(2)}_{yxy} = \chi^{(2)}_{zxz}$. We set $\rho_{fib} = \frac{\chi^{(2)}_{xxx}}{\chi^{(2)}_{xzz}}$, called the fibril anisotropy parameter, which has been shown to provide the orientation δ of the peptide bonds to the triple helical axis: $\rho_{fib} = \frac{2}{\tan^2\delta}$ [25,29,36–38].

The SHG signal then depends on 4 independent parameters: the incident polarization angle θ, the fibril orientation angles φ and ψ and the fibril anisotropy parameter ρ_{fib}, besides I_{exc}, $\chi^{(2)}_{xxx}$ and geometrical parameters (excitation and detection numerical apertures, etc. . .) that determine the overall intensity. It is written in the plane wave approximation, without any polarimetric analysis of the SHG signal:

$$I_{SHG} \propto \left(\left| \sum_{J,K} \chi^{(2)}_{XJK} \, E^J_\omega E^K_\omega \right|^2 + \left| \sum_{J,K} \chi^{(2)}_{YJK} \, E^J_\omega E^K_\omega \right|^2 \right). \tag{1}$$

Here J and K stand for X,Y or Z, (XYZ) is the laboratory frame with Z along the microscope optical axis, E^J_ω is the incident electric field along J, depending on the polarization angle θ and $\chi^{(3)}_{IJK}$ is the collagen susceptibility tensor in the laboratory frame, which depends on φ, ψ and ρ_{fib}.

Biomedical Optics EXPRESS

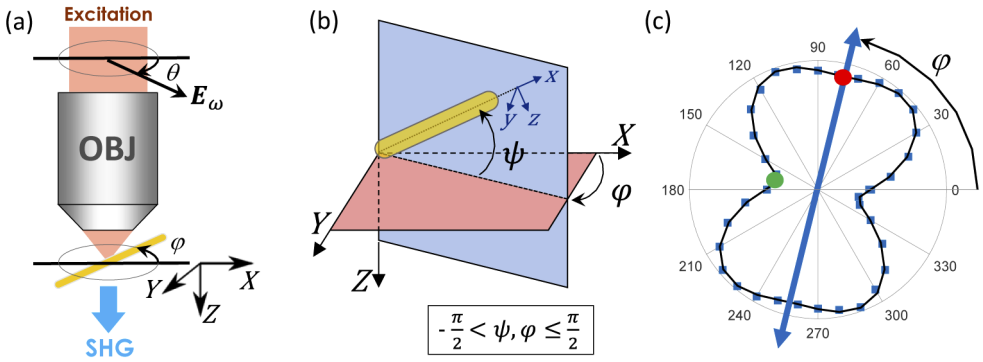

Fig. 2. Principle of P-SHG image acquisition and analysis. (a) Scheme of the P-SHG setup showing the orientation θ of the incident linear polarization and the in-plane orientation φ of the collagen fibril in the laboratory frame (XYZ). (b) Fibril frame (xyz) and orientation of the collagen fibril in the laboratory frame. (c) Experimental (full squares) and theoretical (black line) P-SHG signal as a function of the incident polarization angle θ for a fibril with in-plane orientation φ. The theoretical signal is calculated by inserting the FFT parameters α_0, α_2 and α_4 in Eq. (2). The experimental data have been averaged over several pixels and are therefore in excellent agreement with the theory ($R^2 = 0.99$). The anisotropy parameter corresponds to the square root of the ratio of the SHG signal at φ (red dot) to the one at $\varphi + \pi/2$ (green dot).

One gets [24,28,29,33,39,40]:

$$I_{SHG}(\theta) \;=\; C\, I_{exc}^2 cos^2(\psi)[a_0(\psi) + a_2(\psi)cos(2(\theta-\varphi)) + a_4(\psi)cos(4(\theta-\varphi))]$$

or

$$I_{SHG}(\theta) \;=\; C\, I_{exc}^2 cos^2(\psi)[\alpha_0(\psi) + \alpha_2(\psi)e^{2i\theta} + \alpha_4(\psi)e^{4i\theta} + c.c.] \tag{2}$$

where C is a parameter merging geometrical and other parameters. Equation (2) provides 3 parameters of interest (Fig. 2(c)):

- The mean intensity I_{av} obtained by averaging $I_{SHG}(\theta)$ over all angles θ, which is proportional to $cos^2(\psi)$ and thus maximal for in-plane fibrils:

$$I_{av} \;=\; C\, I_{exc}^2 cos^2(\psi)a_0(\psi). \tag{3}$$

- The in-plane angle φ of the collagen fibrils. It is determined as the weighted average of the angles $\varphi_2 = -\frac{arg(\alpha_2)}{2}$ and $\varphi_4 = -\frac{arg(\alpha_4)\pm\pi}{4}$ [41,42]. It corresponds to the first minimum of the polarimetric diagram $I_{SHG}(\theta)$ (Fig. 2(c)).

- The contrast of the polarimetric diagram $I_{SHG}(\theta)$, defined as the square root of the ratio of the 2 minima: $\rho = \sqrt{\frac{I_{SHG}(\varphi)}{I_{SHG}(\varphi+\pi/2)}}$ (Fig. 2c). It is called the anisotropy parameter in the laboratory frame and obtained as: $\rho = \sqrt{\frac{a_0+a_2+a_4}{a_0-a_2+a_4}}$, assuming that $a_2 \geq 0$ and $a_4 \leq 0$, as verified for collagen. This parameter varies with ρ_{fib} and the out-of-plane angle ψ: $\rho = \rho_{fib}(cos^2\psi + 3sin^2\psi)$[33,39]. It also varies with the orientation dispersion of the fibrils when they are not aligned together within the focal volume [24,25,40,43].

The most relevant parameter in this study is the in-plane angle φ that provides a pixel-wise measure of the orientation of the collagen lamellae with respect to the corneal surface. The distribution of the out-of-plane angle ψ may be deduced from the mean intensity I_{av} and the

Biomedical Optics EXPRESS

anisotropy parameter in the laboratory frame ρ, as previously reported, but this is beyond the scope of this study.

Processing of P-SHG images based on Eq. (2) is performed automatically using custom-written Matlab codes applicable to Z-stacks of P-SHG images. First, a median filter of 2-pixel size is applied to all images in order to increase the signal to noise ratio. Then the parameters α_0, α_2 and α_4 are computed pixel-wise using a Fast Fourier Transform (FFT) of $I_{SHG}(\theta)$. Finally, 2D maps of the mean intensity I_{av}, the in-plane angle φ and the anisotropy parameter ρ are calculated using the method explained above. Thanks to FFT, this method is fast, but it provides a result even if the experimental variation of $I_{SHG}(\theta)$ does not comply with the theoretical model of Eq. (2), for instance at the interface between 2 lamellae where there are fibrils with 2 different orientations within the focal volume. Therefore, in order to verify whether φ and ρ are determined in a reliable way, we compute in every pixel a coefficient of determination R^2 that compares the experimental data $I_{SHG}^{exp}(\theta)$ to the data $I_{SHG}^{FFT}(\theta)$ obtained by inserting the parameters α_0, α_2 and α_4 in Eq. (2) (Fig. 2(c)). The in-plane angle φ maps are then displayed using an HSV look-up table: the hue (H) codes the orientation, the saturation (S) codes the R^2 and the value (or brightness) codes the mean intensity I_{av}.

2.5. Automatic quantitative processing of lamellae inclination in the anterior stroma

The first set of P-SHG images is processed to obtain the mean lamellae inclination with respect to the cornea surface in the most anterior region of the stroma, which is defined here as within 30 µm from the Bowman's membrane (Fig. 1(b)). Accordingly, the P-SHG tiles are cropped to keep only a 30-µm thick region of the stroma below the Bowman's membrane, which is filtered out. An average of the angle φ is first calculated in every cropped tile along the epithelium and corrected by the orientation of the Bowman's membrane in this tile. Then the mean angles φ are averaged again in all the images acquired along the epithelium and the tiles are stitched together to get a wider field of view. Note that the keratoconic cornea K4 is discarded from this analysis because its surface is too wavy to serve as a reference orientation.

Noteworthy, the P-SHG images are processed pixel-by-pixel without any segmentation of the lamellae. The average is calculated either over all pixels with $R^2 \geq 0.4$ or after the application of a threshold based on the moments of the intensity distribution [44]. The latter method selects the pixels with the highest SHG signal, which corresponds to fibrils with small out-of-plane angles ψ as shown by Eq. (3).

2.6. Automatic quantitation of disorder parameters of the collagen orientation distribution in the anterior, middle, posterior and full stroma

The second set of P-SHG images is used to assess the parallel organization of collagen lamellae within the stroma. The orientation angles φ that are obtained with $R^2 < 0.4$ are filtered out and histograms of the remaining angles are computed in the full stroma and in the anterior, middle and posterior stroma. The lamellae distributions are then quantified by calculating the normalized entropy S of these angular distributions $p(\varphi)$ [45,46]. S is defined as the usual statistical entropy, using angular bins of 10°, and is normalized to be independent of the number of bins $nb(\varphi)$.

$$S = \frac{-1}{\ln[nb(\varphi)]} \sum_{\varphi=-90^\circ}^{90^\circ} p(\varphi)\ln[p(\varphi)]. \tag{4}$$

Thus, $S = 1$ represents an isotropic distribution, while S decreases for a more ordered distribution, where the fibrils are aligned along one or several main orientations. Alternatively, as the angle distribution shows a maximum (see below, Fig. 6), which indicates a main orientation at an angle φ_{main}, we can calculate the orientation index OI [45,46], which is defined as the

Biomedical Optics EXPRESS

percentage of fibrils that are aligned along this main orientation φ_{main}:

$$OI = \left[2\left(\frac{\int_{-90°}^{90°} p(\varphi)cos^2(\varphi - \varphi_{main})d\varphi}{\int_{-90°}^{90°} p(\varphi)d\varphi}\right) - 1\right] \times 100. \quad (5)$$

This *OI* vanishes for an isotropic distribution and is equal to 100% when all the lamellae exhibit the same orientation. Noteworthy, here again, the entropy and the *OI* are calculated for the pixel-by-pixel distribution of orientation angles in the imaging plane, without any segmentation of the lamellae.

2.7. Statistical analysis

The 8 control corneas and the 6 keratoconic corneas are compared by a two-tailed Student test with Welch's approximation. A p-value less than 0.05 is considered as significant. * means $p<0.05$, ** means $p<0.01$, NS means "non-significant". Box plots show the quartiles (box) and the median (horizontal line).

3. Results

3.1. Ultrastructural imaging of lamellae using TEM

Ultrastructural imaging of control corneas by TEM shows well-aligned collagen fibrils at a fixed distance from each other within regularly stacked lamellae as expected from the literature (Fig. 3(a)). In contrast, in keratoconic corneas, alterations in the stromal architecture are clearly visible by breaks within the lamellae, less collagen fibrils as well as changes in the distances and orientations of the collagen fibrils within the lamellae (Fig. 3(b)). The electron micrographs with the most severe disruptions of the lamellar organization were taken close to the cone associated with the pathology. However, changes in the lamellar organization were also clearly observed outside of the cone.

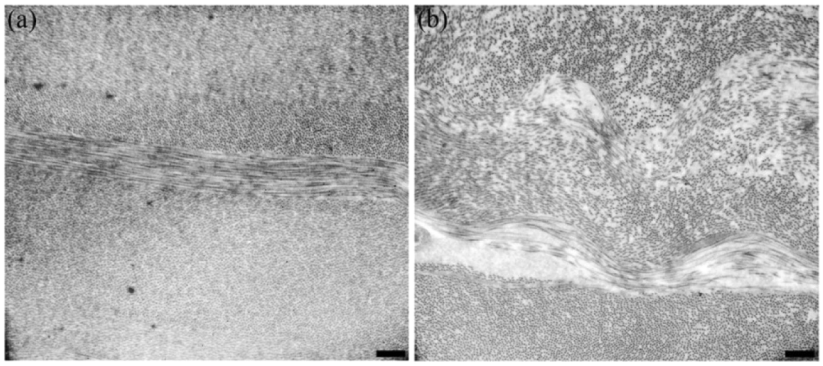

Fig. 3. Typical TEM images of transverse sections of (a) control (C1) and (b) keratoconic (K1) human corneas, in the middle stroma. The sections are orientated with the epithelium side at the top. Scale bars: 1 µm.

3.2. Structural imaging of lamellae distribution using P-SHG

P-SHG microscopy was used to visualize the lamellae disorganization of keratoconic corneas over a larger field of view than in TEM. First, we acquired large P-SHG images of the most anterior region of the stroma by stitching several tiles recorded sequentially along the entire epithelium of the cornea section. Depending on the size of every cornea section, we obtained

Biomedical Optics EXPRESS

images covering 0.4 to 1.9 mm along the cornea width. Figure 4 shows single-tile images of the same control and keratoconic corneas as in Fig. 3. The stitched images of the very anterior side of the 8 control and 6 keratoconic corneas are displayed in Fig. 5. Second, we acquired large P-SHG images of the full stroma thickness by stitching several tiles recorded sequentially all along the stroma. Depending on the size of every stroma, we obtained images showing the stroma over a thickness of 0.68 to 1.11 mm. This thickness variability may be attributed to the combined effects of the intrinsic thickness variability among corneas from different patients, a slightly oblique cutting instead of perfect transverse cutting of the sections, and the onset of slight edema during corneal handling before fixation. Figure 6 shows the P-SHG images acquired in the same control and keratoconic corneas as in Figs. 3 and 4, and Fig. 7 shows the P-SHG images of all the control and keratoconic corneas.

As a polarimetric technique, P-SHG microscopy provides in every pixel the average direction of the collagen fibrils within the imaging plane. P-SHG images display this orientation as a color according to the color wheel displayed in the insets. As expected, the lamellae are mostly oriented parallel to the cornea surface, which corresponds to green- and blueish colors because the corneal epithelium is always oriented along the X axis (φ=0°) for SHG imaging [1]. However, some lamellae are inclined with respect to the cornea surface (red- and yellowish colors). These so-called sutural or transverse lamellae are mainly found in the anterior stroma in agreement

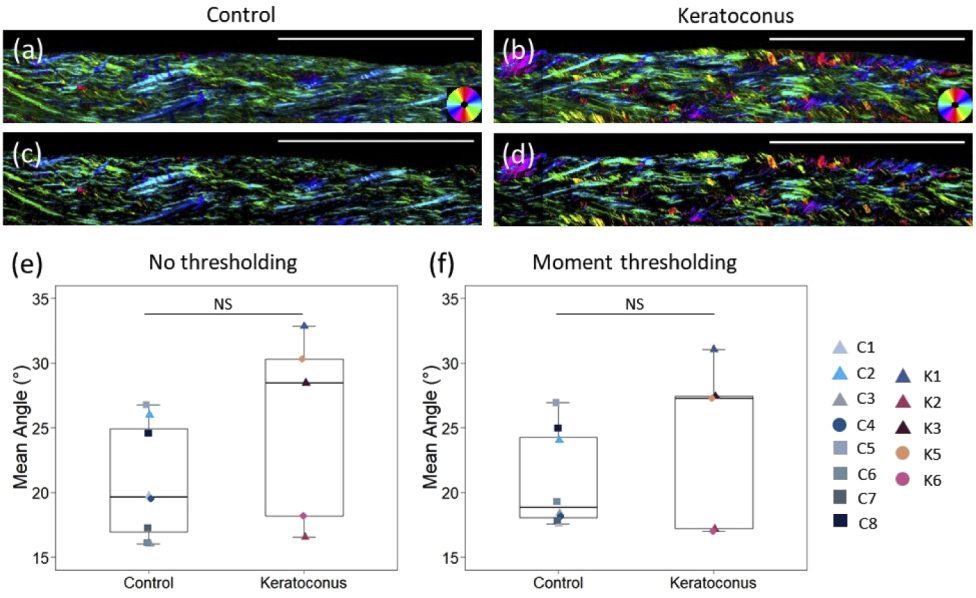

Fig. 4. Anterior lamellae inclination to the corneal surface in control and keratoconic corneas. (a-d) Typical orientation maps obtained from P-SHG imaging in control (a, c) and keratoconic (b, d) corneas, without (a, b) and with (c, d) moment thresholding. The control (C1) and keratoconic (K1) corneas are the same as in Fig. 3. The color wheel of the HSV look-up-table is indicated in the inset. Scale bars: 100 µm. (e, f) Mean lamellae inclination with respect to the corneal surface of control versus keratoconic corneas (e) without any thresholding and (f) with moment thresholding. The mean lamellae inclination of every cornea is obtained as the pixel-wise average of the angles determined in ≈ 6 orientation maps of the anterior stroma (within 30 µm from the Bowman's membrane) recorded along the corneal epithelium and tiled together. Both methods (without or with moment thresholding) show no statistical difference between control and keratoconic corneas.

Biomedical Optics EXPRESS

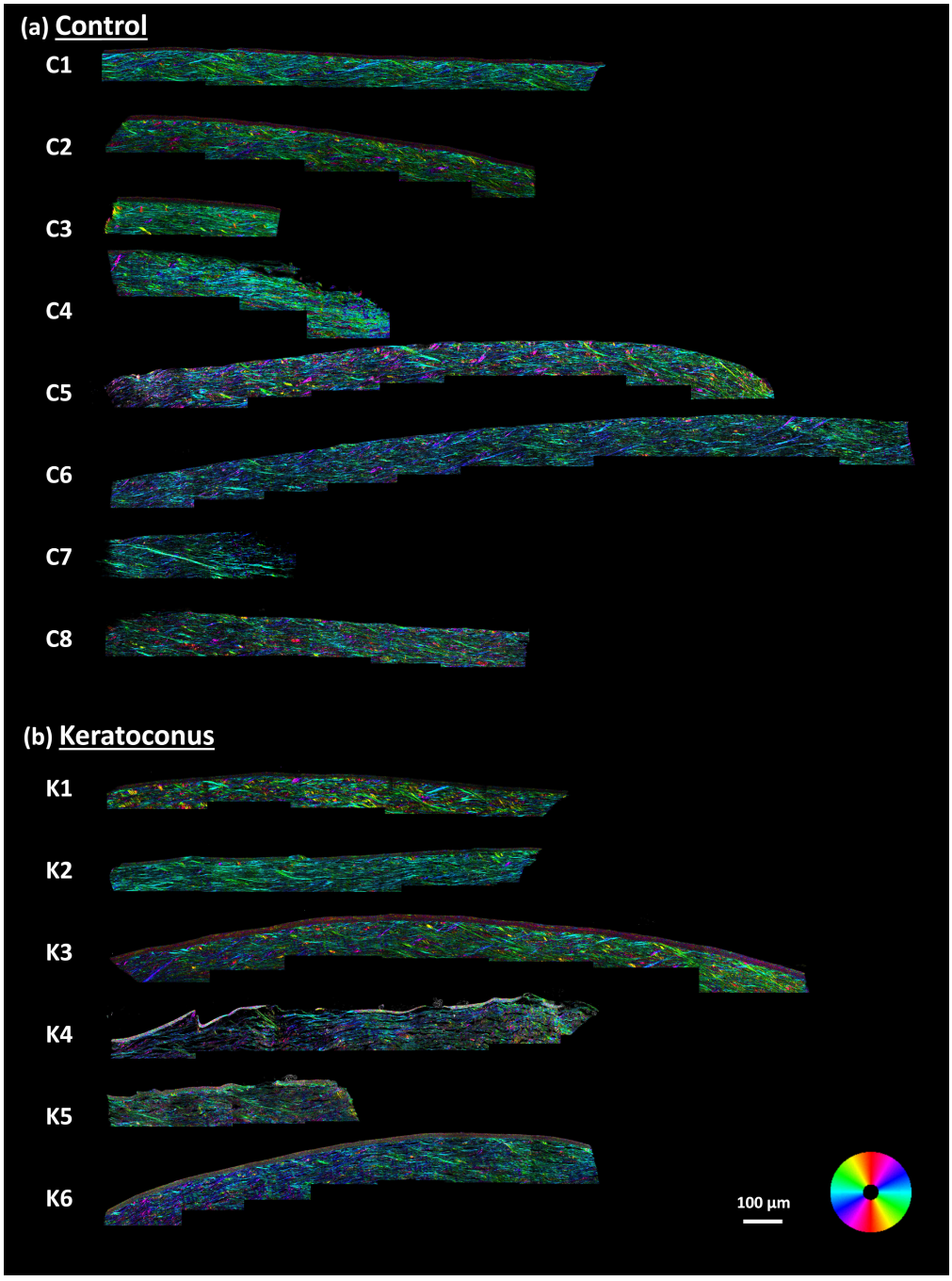

Fig. 5. Orientation maps obtained from P-SHG imaging of the most anterior part of the stroma of (a) control and (b) keratoconic corneas. The color wheel of the HSV look-up-table is indicated in the inset.

Biomedical Optics EXPRESS

with previous reports [3,4,7]. They are found both in the control and in the keratoconic corneas (Figs. 4(a)-(b) and 5). Regarding the organization of the whole stroma, the lamellae of the keratoconic corneas appear somewhat disorganized compared to the ones of the control corneas (Figs. 6(a)-(b) and 7), as visualized by the wider range of colors. To confirm these qualitative observations, we have implemented quantitative processing of P-SHG images to measure the average lamellae inclination in the anterior stroma and order parameters in the full stroma.

3.3. Lamellae inclination in the anterior stroma

Figures 4(e) and 4(f) display the mean lamellae inclination to the cornea surface in the most anterior stroma of every cornea. All data are listed in Supplement 1 (Table S1). In Fig. 4(e), the average is calculated over all pixels where the orientation is determined in a reliable way ($R^2 \geq 0.4$, Figs. 4(a)-(b)). However, the inclination may be over-estimated in lamellae that are oriented out of the imaging plane because the φ angle is a projection of the inclination on the imaging-plane. To

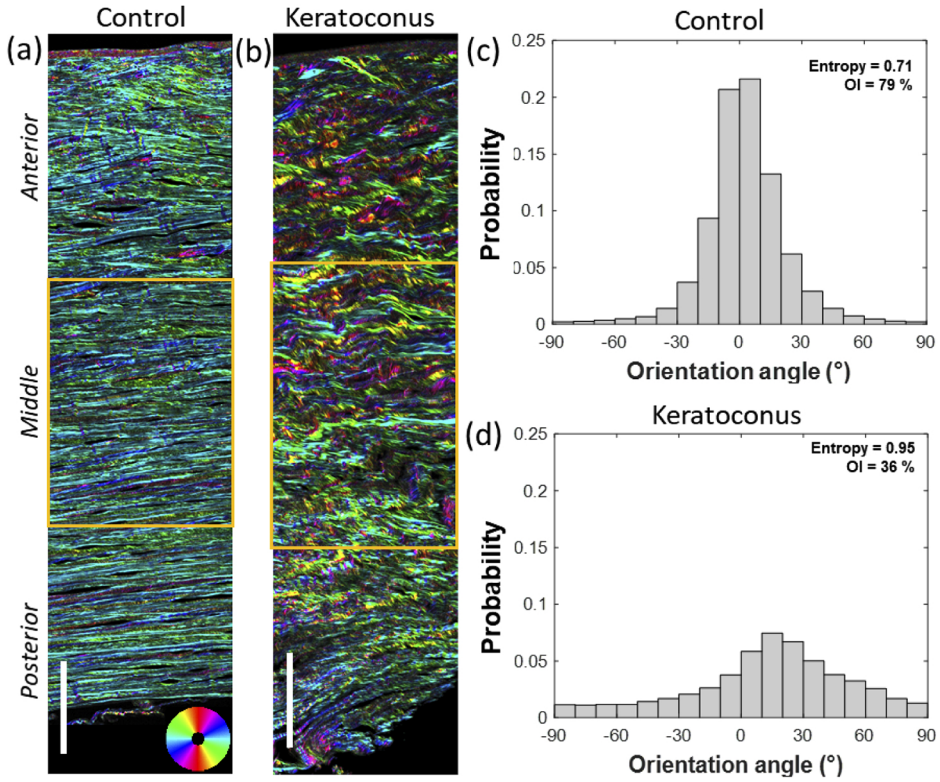

Fig. 6. Orientation distribution of collagen lamellae in control and keratoconic corneas. (a, b) Typical orientation maps obtained from P-SHG images of transverse sections of the same control (a, C1) and keratoconic (b, K1) human corneas as in Figs. 3 and 4, using HSV look-up table. H (hue): collagen orientation according to the color wheel displayed as inset, S (saturation): coefficient of determination R^2 of P-SHG image processing and V (value or brightness): SHG signal. Scale bars: 100 µm. (c, d) Histograms of the collagen orientation in the middle stroma of the (c) control and (d) keratoconic corneas displayed in (a, b). The orientations are computed pixel-wise in the ROIs outlined in yellow. The entropy (resp. the orientation index) of the distributions are indicated in the graphs and show a higher (resp. smaller) value for the keratoconic cornea in agreement with the more diverse colors observed in the orientation map.

Biomedical Optics EXPRESS

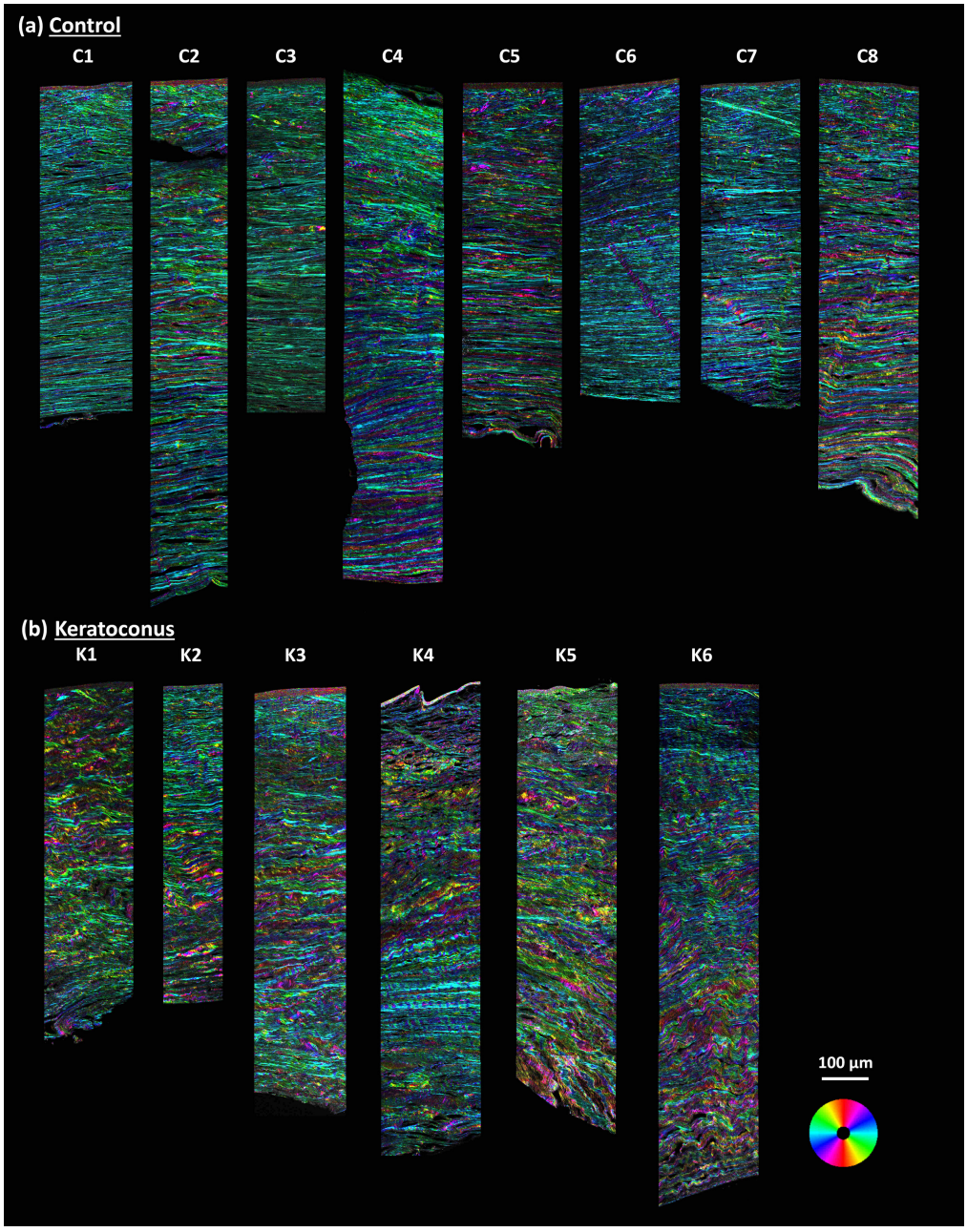

Fig. 7. Orientation maps obtained from P-SHG imaging of the full thickness of the stroma of (a) control and (b) keratoconic corneas. The color wheel of the HSV look-up-table is indicated in the inset.

Biomedical Optics EXPRESS

address this issue, a moment threshold is used to select only the pixels with the highest SHG signal, which correspond to in-plane lamellae as shown by Eq. (3) (Figs. 4(c)-(d)). Accordingly, the resulting mean inclination angle is slightly smaller than without moment thresholding (Fig. 4(f) and Table S1); it is 22° ± 5° for all control and keratoconic corneas. Nevertheless, whatever the calculation method, the lamellae inclination shows no statistical difference between control and keratoconic corneas, despite the large areas probed with small pixel size along the corneas.

3.4. Order parameters of the lamellae transverse orientation along the stroma

The degree of order of the lamellae orientation distribution along the stroma is assessed from orientation histograms computed from the P-SHG data (Figs. 6(c) and 6(d)). As expected, these histograms peak close to 0°, which corresponds to the direction parallel to the cornea surface. However, the peaks obtained in the keratoconic corneas are wider than the ones in control corneas, which reflects a larger orientation disorder. It is assessed quantitatively by computing the entropy S and the orientation index OI of these orientation histograms: the entropy increases and the orientation index decreases when the disorder increases. All data are listed in Supplement 1 (Table S1). Figure 8(a) shows that the entropy of the keratoconic corneas is significantly larger than the one of the control corneas in all regions (anterior, middle, posterior) of the stroma and in the full stroma. Similarly, Fig. 8(b) shows that the orientation index of the keratoconic corneas is significantly smaller than the one of the control corneas in all regions (anterior, middle, posterior) of the stroma and in the full stroma. Both quantitative parameters thus consistently demonstrate that keratoconic corneas exhibit a more disordered distribution of collagen lamellae than control corneas all along the stroma.

4. Discussion

The increasing incidence of keratoconus has prompted many studies aiming at characterizing the modifications of the corneal structure and ultrastructure related to this pathology. Our TEM images show that the fibril alignment within lamellae and the lamellae organization are disrupted in keratoconic corneas, in agreement with previous reports [13,14]. However, the field of view of TEM imaging is quite small ($\leq 10 \times 10$ µm^2), which impedes any extensive characterization of all regions of the corneal stroma. Further studies are needed to provide a quantitative assessment of the stromal disorder in keratoconus over the full depth of the stroma instead of qualitative observations in small regions of interest. In this respect, SHG microscopy, as an optical imaging technique, provides a larger field of view ($> 500 \times 500$ µm^2). While TEM remains the only technique providing ultrastructural imaging of the fibril organization within the lamellae, the sub-micrometer resolution (≈ 0.4 µm) of SHG microscopy is sufficient to characterize the stromal lamellar organization. However, usual SHG imaging poorly discriminates neighboring lamellae that exhibit similar SHG signal in transverse corneal sections. Likewise, the limited axial resolution (1 to 2 µm) compromises the detection of the thinnest lamellae (≤ 1 µm) by *en face* imaging of intact corneas.

In this study, we use P-SHG microscopy to overcome these limitations thanks to the high sensitivity of polarimetric measurements to the fibril anisotropy. The main advantage of this technique is to provide a direct and accurate measure of the collagen orientation in the imaging plane in every pixel of the image, without any image processing that degrades the resolution nor any segmentation step that may introduce bias. Consequently P-SHG provides robust data averaged over a large number of pixels. Then, our implementation of an automatic data processing to obtain unbiased quantitative parameters of interest provides an efficient method to assess the stromal structural modifications in keratoconus.

We first focus on the anterior stroma and use a small pixel size to accurately measure the inclination angle of sutural lamellae. We observe no significant difference between control and keratoconic corneas, which disagrees with previous studies that have reported a smaller

Biomedical Optics EXPRESS

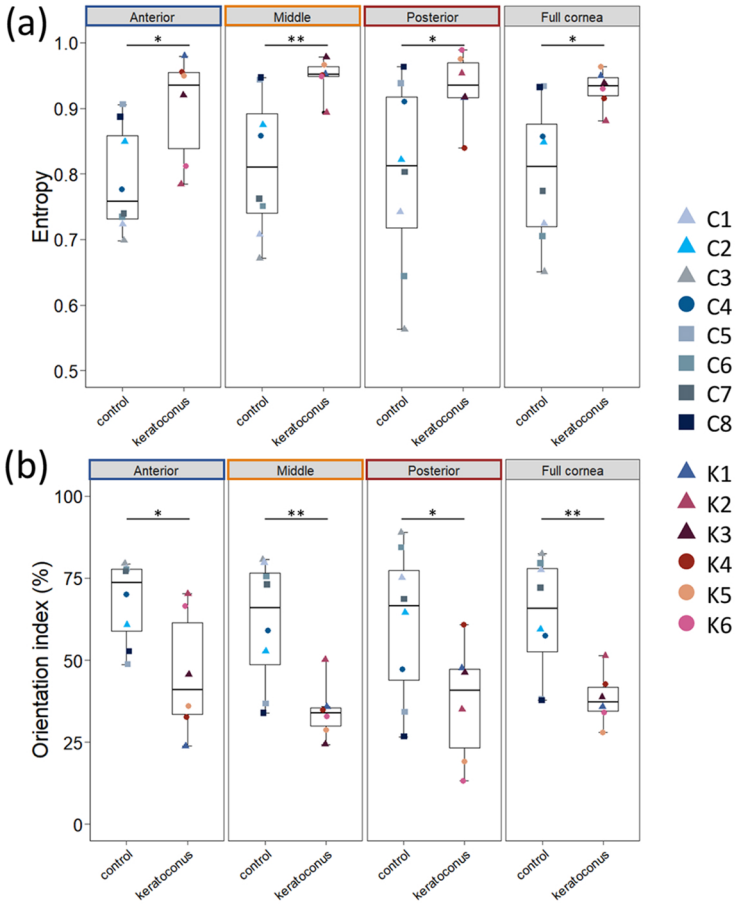

Fig. 8. Quantitative assessment of collagen orientation distribution in control versus keratoconic human corneas. (a) Entropy and (b) orientation index of the orientation distribution in the anterior stroma, middle stroma, posterior stroma and full stroma (from left to right).

inclination in keratoconic corneas [17,18,20]. It may be attributed to the difference in the methods used to calculate the mean inclination angle that rely, in all previous studies, on image processing rather than on P-SHG. Moreover, most previous reports perform a manual segmentation of individual lamellae and average the inclination angles over these segmented lamellae [17,20]. In contrast, our method is a fully automated method based on a pixel-by-pixel calculation followed by an average over these pixels to avoid the segmentation of the lamellae, which may be biased. In addition, because of this average at pixel scale, our method provides the mean inclination of the lamellae weighted by the surface of every lamella in the field of view, which may be different from the unweighted average.

We next examine the degree of disorder of stromal lamellae in keratoconus. Our method combining P-SHG and automatic quantitative analysis provides a rigorous demonstration of increased lamellar disorder in all regions of keratoconic corneas (Fig. 8). This result is in good agreement with the TEM observations at a smaller scale, which show a disruption of the well-ordered distribution of the collagen fibrils within every lamella, with changes in the distance and relative orientation of the fibrils and even breaks of lamellae (Fig. 3(b)). It shows that the

Biomedical Optics EXPRESS

disruption of the collagen organization in keratoconic corneas is a multi-scale process that affects both the alignment of fibrils within the lamellae and the inter-lamellae alignment along the full stroma. This agrees with previous reports that also evidenced a disorganization of the stroma of keratoconic corneas [15,19,47]. However, these previous reports performed "*en-face*" imaging by use of X-rays or SHG microscopy and thus probed the orientation distribution in a plane parallel to the cornea surface. In this study, P-SHG and TEM images are recorded on transverse sections, so that they probe the orientation distribution in a transverse plane with respect to the cornea surface, in a complementary way to the previous reports. Moreover, our study provides quantitative measurements in all the regions of the stroma, which is challenging to achieve with other techniques. It shows that P-SHG microscopy provides an enhanced sensitivity to the stromal lamellar organization compared to other imaging techniques.

The disorder exhibited by the keratoconic corneas is consistent with the deteriorated mechanical behavior observed by clinicians. Numerical models of the cornea mechanical response have indeed shown that the well-ordered lamellae structure is crucial to provide cornea with enough rigidity to compensate for intraocular pressure and external shocks [48,49]. An interesting perspective of this study would be to supply these numerical models with the disorder parameters measured in keratoconic corneas. It would enable the construction of advanced numerical models that fully take into account the cornea lamellar structure and a better prediction of the mechanical consequences of any structural disorder. In this respect, the unique capability of our method to provide quantitative data in different regions of the cornea is critical.

P-SHG microscopy coupled to automatic data processing could also be used to study preliminary stages of keratoconus or other structural disorders that may be characterized by heterogeneous structural modifications of the stroma. Another interesting perspective would be to study corneal healing after refractive surgery or any injury. We indeed expect that the cornea does not perfectly recover and keeps a distorted structure for a long time, which should be quantitatively characterized to assess the efficiency of various treatments. It is worth noting that all these studies would require a large number of corneal samples, which may be a limitation regarding human samples and may require to use animal models. Nevertheless, the fully automation of our image processing method, with no manual adjustment of parameters, enables to increase the number of samples by merging data from several clinical centers, which is a unique advantage for little number of samples.

5. Conclusion

This study shows that P-SHG microscopy enables a quantitative analysis of the lamellar structure of healthy and keratoconic corneas. Our data on transverse sections demonstrate unambiguously that the lamellae orientation distribution is wider in keratoconic corneas than in control ones, corresponding to a loss of order in the lamellar structure. Most importantly, this method requires no segmentation of the lamellae and provides the collagen orientation in every pixel in a fully automated way, without the need to adjust any parameter. This makes P-SHG microscopy a very sensitive and reliable method to analyze the orientation disorder in keratoconic corneas. This method could be judiciously implemented in further studies to analyze other corneal structural pathologies, as well as other collagen-rich organs that exhibit a highly organized structure at the micrometer scale, such as bones, cartilages or tendons.

Funding. Agence Nationale de la Recherche (ANR-10-INBS-04, ANR-11-EQPX-0029).

Acknowledgments. The authors thank Xavier Solinas and Jean-Marc Sintès for technical support in the SHG setup, and the "Advanced microscopies and tissue physiology" group at LOB for fruitful discussions. We thank Karin Gäher for excellent technical support.

Disclosures. The authors declare no conflicts of interest.

Data availability. All the P-SHG images underlying the quantitative analyses are displayed in the article. All the data underlying the results presented in Figs. 4 and 8 are provided in the Supplementary table S1.

Biomedical Optics EXPRESS

Supplemental document. See Supplement 1 for supporting content.

References

1. K. M. Meek and C. Knupp, "Corneal structure and transparency," Prog. Retinal Eye Res. **49**, 1–16 (2015).
2. S. Hayes, C. Boote, J. Lewis, J. Sheppard, M. Abahussin, A. J. Quantock, C. Purslow, M. Votruba, and K. M. Meek, "Comparative study of fibrillar collagen arrangement in the corneas of primates and other mammals," Anat. Rec. **290**(12), 1542–1550 (2007).
3. N. Morishige, Y. Takagi, T. Chikama, A. Takahara, and T. Nishida, "Three-dimensional analysis of collagen lamellae in the anterior stroma of the human cornea visualized by second harmonic generation imaging microscopy," Invest. Ophthalmol. Visual Sci. **52**(2), 911–915 (2011).
4. M. Winkler, G. Shoa, Y. L. Xie, S. J. Petsche, P. M. Pinsky, T. Juhasz, D. J. Brown, and J. V. Jester, "Three-dimensional distribution of transverse collagen fibers in the anterior human corneal stroma," Invest Ophth Vis Sci **54**(12), 7293–7301 (2013).
5. A. J. Quantock, M. Winkler, G. J. Parfitt, R. D. Young, D. J. Brown, C. Boote, and J. V. Jester, "From nano to macro: Studying the hierarchical structure of the corneal extracellular matrix," Exp. Eye Res. **133**, 81–99 (2015).
6. K. Grieve, D. Ghoubay, C. Georgeon, G. Latour, A. Nahas, K. Plamann, C. Crotti, R. Bocheux, M. Borderie, T.-M. Nguyen, F. Andreiuolo, M.-C. Schanne-Klein, and V. Borderie, "Stromal striae: a new insight into corneal physiology and mechanics," Sci. Rep. **7**(1), 13584 (2017).
7. A. Abass, S. Hayes, N. White, T. Sorensen, and K. M. Meek, "Transverse depth-dependent changes in corneal collagen lamellar orientation and distribution," J. R. Soc. Interface. **12**(104), 20140717 (2015).
8. A. Gautieri, S. Vesentini, A. Redaelli, and M. J. Buehler, "Hierarchical structure and nanomechanics of collagen microfibrils from the atomistic scale up," Nano Lett. **11**(2), 757–766 (2011).
9. A. Benoit, G. Latour, M.-C. Schanne-Klein, and J.-M. Allain, "Simultaneous microstructural and mechanical characterization of human corneas at increasing pressure," J. Mech. Behav. Biomed. Mater. **60**, 93–105 (2016).
10. J. S. Bell, S. Hayes, C. Whitford, J. Sanchez-Weatherby, O. Shebanova, C. Vergari, C. P. Winlove, N. Terrill, T. Sorensen, A. Elsheikh, and K. M. Meek, "The hierarchical response of human corneal collagen to load," Acta Biomater. **65**, 216–225 (2018).
11. H. Hashemi, S. Heydarian, E. Hooshmand, M. Saatchi, A. Yekta, M. Aghamirsalim, M. Valadkhan, M. Mortazavi, A. Hashemi, and M. Khabazkhoob, "The prevalence and risk factors for keratoconus: a systematic review and meta-analysis," Cornea **39**(2), 263–270 (2020).
12. H. R. Vellara and D. V. Patel, "Biomechanical properties of the keratoconic cornea: a review," Clin Exp Optom **98**(1), 31–38 (2015).
13. S. Akhtar, A. J. Bron, S. M. Salvi, N. R. Hawksworth, S. J. Tuft, and K. M. Meek, "Ultrastructural analysis of collagen fibrils and proteoglycans in keratoconus," Acta Ophthalmol **86**(7), 764–772 (2008).
14. A. Alkanaan, R. Barsotti, O. Kirat, T. Almubrad, A. Khan, and S. Akhtar, "Ultrastructural study of peripheral and central stroma of keratoconus cornea," Br. J. Ophthalmol. **101**(6), 845–850 (2017).
15. K. M. Meek, S. J. Tuft, Y. F. Huang, P. S. Gill, S. Hayes, R. H. Newton, and A. J. Bron, "Changes in collagen orientation and distribution in keratoconus corneas," Invest. Ophthalmol. Visual Sci. **46**(6), 1948–1956 (2005).
16. H. Y. Tan, Y. Sun, W. Lo, S. J. Lin, C. H. Hsiao, Y. F. Chen, S. C. Huang, W. C. Lin, S. H. Jee, H. S. Yu, and C. Y. Dong, "Multiphoton fluorescence and second harmonic generation imaging of the structural alterations in keratoconus ex vivo," Invest. Ophthalmol. Visual Sci. **47**(12), 5251–5259 (2006).
17. N. Morishige, R. Shin-gyou-uchi, H. Azumi, H. Ohta, Y. Morita, N. Yamada, K. Kimura, A. Takahara, and K. H. Sonoda, "Quantitative analysis of collagen lamellae in the normal and keratoconic human cornea by second harmonic generation imaging microscopy," Invest Ophth Vis Sci **55**(12), 8377–8385 (2014).
18. R. Mercatelli, F. Ratto, F. Rossi, F. Tatini, L. Menabuoni, A. Malandrini, R. Nicoletti, R. Pini, F. S. Pavone, and R. Cicchi, "Three-dimensional mapping of the orientation of collagen corneal lamellae in healthy and keratoconic human corneas using SHG microscopy," J. Biophoton **10**(1), 75–83 (2017).
19. A. Batista, H. G. Breunig, A. Konig, A. Schindele, T. Hager, B. Seitz, and K. Konig, "High-resolution, label-free two-photon imaging of diseased human corneas," J. Biomed. Opt. **23**(03), 1 (2018).
20. E. Mikula, M. Winkler, T. Juhasz, D. J. Brown, G. Shoa, S. Tran, M. C. Kenney, and J. V. Jester, "Axial mechanical and structural characterization of keratoconus corneas," Exp. Eye Res. **175**, 14–19 (2018).
21. G. Scarcelli, S. Besner, R. Pineda, and S. H. Yun, "Biomechanical characterization of keratoconus corneas ex vivo with Brillouin microscopy," Invest. Ophthalmol. Visual Sci. **55**(7), 4490–4495 (2014).
22. F. Aptel, N. Olivier, A. Deniset-Besseau, J.-M. Legeais, K. Plamann, M.-C. Schanne-Klein, and E. Beaurepaire, "Multimodal nonlinear imaging of the human cornea," Invest. Ophthalmol. Vis. Sci **51**(5), 2459–2465 (2010).
23. M. Winkler, G. Shoa, S. T. Tran, Y. L. Xie, S. Thomasy, V. K. Raghunathan, C. Murphy, D. J. Brown, and J. V. Jester, "A comparative study of vertebrate corneal structure: the evolution of a refractive lens," Invest. Ophthalmol. Vis. Sci. **56**(4), 2764–2772 (2015).
24. A. E. Tuer, M. K. Akens, S. Krouglov, D. Sandkuijl, B. C. Wilson, C. M. Whyne, and V. Barzda, "Hierarchical model of fibrillar collagen organization for interpreting the second-order susceptibility tensors in biological tissue," Biophys. J. **103**(10), 2093–2105 (2012).
25. I. Gusachenko, Y. Goulam Houssen, V. Tran, J.-M. Allain, and M.-C. Schanne-Klein, "Polarization-resolved second-harmonic microscopy in tendon upon mechanical stretching," Biophys. J. **102**(9), 2220–2229 (2012).

Biomedical Optics EXPRESS

26. C. A. Couture, S. Bancelin, J. Van der Kolk, K. Popov, M. Rivard, K. Legare, G. Martel, H. Richard, C. Brown, S. Laverty, L. Ramunno, and F. Legare, "The Impact of Collagen Fibril Polarity on Second Harmonic Generation Microscopy," Biophys. J. **109**(12), 2501–2510 (2015).
27. M. Schmeltz, C. Teulon, M. Pinsard, U. Hansen, M. Alnawaiseh, D. Ghoubay, V. Borderie, G. Mosser, C. Aimé, G. Latour, and M.-C. Schanne-Klein, "Circular Dichroism-SHG microscopy probes the polarity distribution of collagen fibrils," Optica **7**(11), 1469–1476 (2020).
28. P. Stoller, K. M. Reiser, P. M. Celliers, and A. M. Rubenchik, "Polarization-modulated second harmonic generation in collagen," Biophys J. **82**(6), 3330–3342 (2002).
29. J. Duboisset, D. Ait-Belkacem, M. Roche, H. Rigneault, and S. Brasselet, "Generic model of the molecular orientational distribution probed by polarization-resolved second-harmonic generation," Phys. Rev. A **85**(4), 043829 (2012).
30. G. Latour, I. Gusachenko, L. Kowalczuk, I. Lamarre, and M.-C. Schanne-Klein, "*In vivo* structural imaging of the cornea by polarization-resolved Second Harmonic microscopy," Biomed. Opt. Express **3**(1), 1 (2012).
31. M. Lombardo, D. Merino, P. Loza-Alvarez, and G. Lombardo, "Translational label-free nonlinear imaging biomarkers to classify the human corneal microstructure," Biomed. Opt. Express **6**(8), 2803–2818 (2015).
32. J. H. Mathew, J. D. Goosey, and J. P. Bergmanson, "Quantified histopathology of the keratoconic cornea," Optom Vis Sci **88**(8), 988–997 (2011).
33. C. Teulon, A. Tidu, F. Portier, G. Mosser, and M.-C. Schanne-Klein, "Probing the 3D structure of cornea-like collagen liquid crystals with polarization-resolved SHG microscopy," Opt. Express **24**(14), 16084–16098 (2016).
34. R. W. Boyd, *Nonlinear Optics* (Academic Press, 2003).
35. S. Roth and I. Freund, "Second harmonic generation in collagen," J. Chem. Phys. **70**(4), 1637–1643 (1979).
36. S. V. Plotnikov, A. C. Millard, P. J. Campagnola, and W. A. Mohler, "Characterization of the myosin-based source for second-harmonic generation from muscle sarcomeres," Biophys. J. **90**(2), 693–703 (2006).
37. F. Tiaho, G. Recher, and D. Rouède, "Estimation of helical angle of myosin and collagen by second harmonic generation imaging microscopy," Opt. Express **15**(19), 12286–12295 (2007).
38. A. E. Tuer, S. Krouglov, N. Prent, R. Cisek, D. Sandkuijl, K. Yasufuku, B. C. Wilson, and V. Barzda, "Nonlinear optical properties of type i collagen fibers studied by polarization dependent second harmonic generation microscopy," J. Phys. Chem. B **115**(44), 12759–12769 (2011).
39. S. Psilodimitrakopoulos, I. Amat-Roldan, P. Loza-Alvarez, and D. Artigas, "Effect of molecular organization on the image histograms of polarization SHG microscopy," Biomed. Opt. Express **3**(10), 2681–2693 (2012).
40. D. Rouede, E. Schaub, J. J. Bellanger, F. Ezan, J. C. Scimeca, G. Baffet, and F. Tiaho, "Determination of extracellular matrix collagen fibril architectures and pathological remodeling by polarization dependent second harmonic microscopy," Sci. Rep. **7**(1), 12197 (2017).
41. V. Wasik, P. Refregier, M. Roche, and S. Brasselet, "Precision of polarization-resolved second harmonic generation microscopy limited by photon noise for samples with cylindrical symmetry," J. Opt. Soc. Am. A **32**(8), 1437–1445 (2015).
42. M. Pinsard, S. Laverty, H. Richard, J. Dubuc, M.-C. Schanne-Klein, and F. Légaré, "Maturation of the meniscal collagen structure revealed by polarization-resolved and directional second harmonic generation microscopy," Sci. Rep. **9**(1), 18448 (2019).
43. E. I. Romijn, A. Finnoy, and M. B. Lilledahl, "Analyzing the feasibility of discriminating between collagen types I and II using polarization-resolved second harmonic generation," J. Biophotonics **12**(1), e201800090 (2019).
44. W.-H. Tsai, "Moment-preserving thresholding: a new approach," Comput. Vis. Graph. Image Process. **29**(3), 377–393 (1985).
45. C. Bayan, J. M. Levitt, E. Miller, D. Kaplan, and I. Georgakoudi, "Fully automated, quantitative, noninvasive assessment of collagen fiber content and organization in thick collagen gels," J. Appl. Phys. **105**(10), 102042 (2009).
46. S. Bancelin, B. Lynch, C. Bonod-Bidaud, G. Ducourthial, S. Psilodimitrakopoulos, P. Dokladal, J.-M. Allain, M.-C. Schanne-Klein, and F. Ruggiero, "Ex vivo multiscale quantitation of skin biomechanics in wild-type and genetically-modified mice using multiphoton microscopy," Sci. Rep. **5**(1), 17635 (2015).
47. A. Daxer and P. Fratzl, "Collagen fibril orientation in the human corneal stroma and its implication in keratoconus," Invest. Ophthalmol. Visual Sci. **38**, 121–129 (1997).
48. H. Studer, X. Larrea, H. Riedwyl, and P. Buchler, "Biomechanical model of human cornea based on stromal microstructure," J. Biomech. **43**(5), 836–842 (2010).
49. A. Montanino, A. Gizzi, M. Vasta, M. Angelillo, and A. Pandolfi, "Modeling the biomechanics of the human cornea accounting for local variations of the collagen fibril architecture," Z. Angew. Math. Mech. **98**(12), 2122–2134 (2018).